Journal of Alloys and Compounds 582 (2014) 141–145

Contents lists available at ScienceDirect

Journal of Alloys and Compounds

journal homepage: www.elsevier.com/locate/jalcom

Letter

On the nanomechanical characteristics of thermally-treated alloy 690: Grain boundaries versus grain interior

Yakai Zhao, In-Chul Choi, Yong-Jae Kim, Jae-il Jang *

Division of Materials Science & Engineering, Hanyang University, Seoul 133-791, Republic of Korea

ARTICLE INFO

Article history:
Received 19 May 2013
Received in revised form 21 July 2013
Accepted 6 August 2013
Available online 15 August 2013

Keywords:
Alloy 690
Nanoindentation
Grain boundary
Aging

ABSTRACT

Alloy 690 has been widely used as steam generator tubing material in nuclear power plants owing to its excellent properties such as stress corrosion cracking resistance. In the present study, a series of nanoindentation experiments were conducted to explore the nanomechanical characteristics of the grain boundaries (GBs) and grain interior (GI) in the alloy 690 that were isothermally aged for four different times (for simulating the 20–80 years operation under power plant condition). While the accelerated aging induced no pronounced degradation, the GB and GI show remarkable and reproducible differences in nanohardness (plastic flow), pop-in stress (yielding), and strain-rate sensitivity. The results are discussed in terms of dislocation activities in the various mechanisms of deformation behavior.

1. Introduction

Alloy 690, a nickel-based alloy having high chromium contents (up to ~30%), was developed as the replacement for alloy 600 in steam generator tubing of pressurized water reactors (PWRs) in nuclear power plants, and now has been widely used owing to its excellent resistance to stress corrosion cracking (SCC) in aggressive primary water environments at temperatures up to 603 K [1,2]. Since the SCC mechanism is strongly dependent on the structures of grain boundaries (GBs) for a given composition, commercial alloy 690 is typically 'thermally-treated' (so-called TT) at ~988–1005 K for ~5–15 h and thus exhibits significant carbide precipitations formed along random high-angle GBs [1].

In order to ensure the material's long-term reliability under operation environment, extensive research on the aging-induced degradations is essential. In this regard, the GBs has been reported to also play some important role in the possible age degradation mechanisms during operation (such as SCC [3] and intergranular attack [4]), which can be understood by the crystalline incompatibility nature of the GBs. Therefore, analysis of the GBs' mechanical characteristics, especially at the nanoscale, can provide some insights for better understanding of both strengthening and age degradation mechanisms of TT 690. In addition, it is somewhat interesting to note that while nearly all previous studies on the aging of alloy 690 were performed on the solution-annealed (SA) 690 specimens (in which the carbides are dissolved by the solution annealing at ~1293–1423 K for ~1 h) [2–5], but not on the TT 690 specimens.

With these in mind, here we attempted to explore the nanoindentation behavior (that is, nanohardness, yielding stress, and strain rate sensitivity) of the TT 690 specimens for which the accelerated isothermal aging was performed for four different times in consideration of operating condition. To gain some clue for the GBs' role in strengthening and age degradation, we decoupled the target material into GB region and grain interior (GI) region and systematically evaluated the nanomechanical properties of each region.

2. Experimental

Examined material is a commercial grade TT 690 alloy whose nominal composition (in wt%) is 29Cr–10Fe–0.02C–0.3Mn–0.2Si–0.2Ti–0.01Co with the balance Ni. In order to simulate the aging at the average operating temperature of steam generator tubes (~573 K) for target life of 20, 40, 60, and 80 years, the virgin samples were isothermally aged at 648 K for four different times. The "accelerated aging" times were determined based on Larson–Miller parameter (*LMP*), a popular measure for degree of aging [6], that is,

$$LMP = T(\log t + C) \quad (1)$$

where T is the absolute temperature, t is the aging time in hours, and C is a material specific constant (which can be 20 for a Ni-based alloy [7]); i.e., first, the *LMP* values for $T = 573$ K and $t = 20$, 40, 60, and 80 year were calculated by Eq. (1), then equivalent aging times to produce the same *LMP*s for $T = 648$ K were determined as 210, 387, 554, and 715 h, respectively.

Metallurgical examinations were carried out by a field-emission scanning electron microscopy (FE SEM) JSM-340 (JEOL Ltd., Tokyo, Japan) with the samples whose surfaces were mechanically polished with 2000-grit SiC paper and 0.3 μm alumina, and then electrolytically etched at 4 V for 60 s in 6% nital solution in order to reveal GBs for SEM observation.

* Corresponding author. Tel.: +82 222200402; fax: +82 222200389.
E-mail address: jijang@hanyang.ac.kr (J.-i. Jang).

0925-8388/$ - see front matter © 2013 Elsevier B.V. All rights reserved.
http://dx.doi.org/10.1016/j.jallcom.2013.08.044

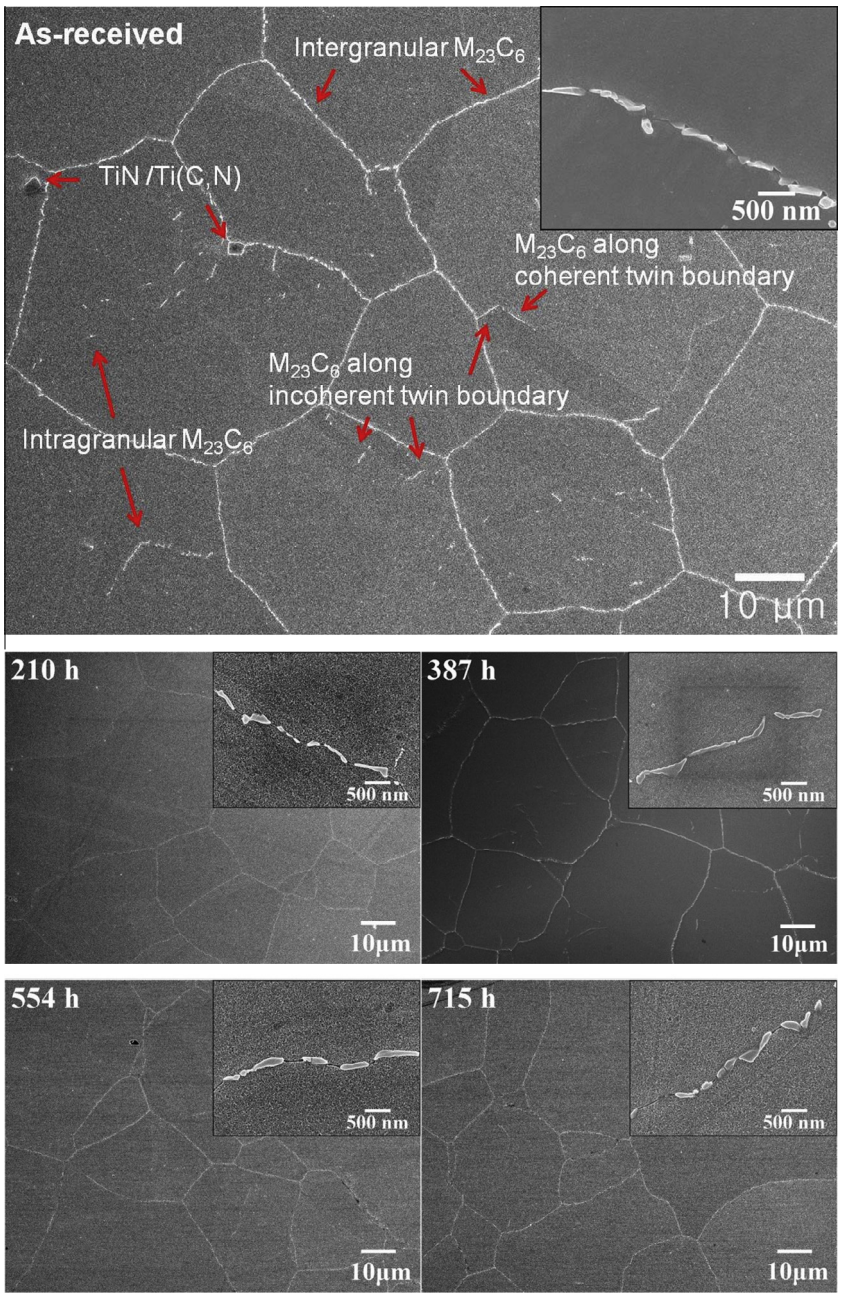

Fig. 1. Representative SEM micrographs of the as-received and isothermally aged specimens. Right-top inset of each image shows the GB precipitates morphologies.

Nanoindentation tests were performed using the Nanoindenter-XP (formerly MTS; now Agilent, Oak Ridge, TN) equipped with two different indenters. First, nanohardness and its rate-sensitivity were estimated with a three-sided pyramidal Berkovich indenter. The hardness calculation and area function calculations were conducted in accordance with Oliver and Pharr method [8]. Second, small-scale yielding behavior was examined with a spherical indenter whose tip radius was verified as 68.5 μm. Before nanoindentation, an electrolytic polishing was conducted at a voltage of 22 V for 20 s in an electrolyte of 20% perchloric acid and 80% ethanol for removing the hardened surface layer (that was induced during mechanical grinding). In addition, this electrolytic polishing induced a slight etching of the GBs, which helped us to find the locations for the nanoindentations on GBs. More than twenty indentations were made for each condition, and the distance between neighboring indentations was set to be always over 4 times the indentation depth.

3. Results and discussion

Representative SEM micrographs of the as-received and aged specimens are shown in Fig. 1. In the as-received (AR) sample, Cr-rich $M_{23}C_6$ precipitates are located along GBs (which is an important feature of TT 690) as well as at either coherent/incoherent twin boundaries or intragranular matrix (probably on dislocations). In addition, a few randomly distributed TiN/Ti(C,N) particles exist in the matrix.

Fig. 1 also exhibits that the accelerated aging adopted here did not alter the microstructures noticeably. The average grain size of the AR specimen was ~30 μm and did not vary remarkably with aging time, which is in a good agreement with previous SA 690 studies [2] where the low-temperature aging treatment barely affects the grain size but mainly induces carbide precipitations. Inset images of Fig. 1 shows typical micrographs of the GB precipitates. Regardless of aging time, the discrete but closely-spaced $M_{23}C_6$ carbide precipitates are located along GBs. The $M_{23}C_6$ carbides were mostly precipitated upon TT processing of this alloy, and almost no carbon was available for additional carbide nucleation during aging. Hence, the carbide morphology can be changed only

by coarsening of precipitates rather than their nucleation. This suggests that no dramatic change in the carbide morphologies is possibly due to the very slow coarsening of pre-existing carbides at the relatively low aging temperature adopted here (~648 K that is higher than operating temperature by only 75 K).

Nanohardness values of the GB and GI were obtained from the nanoindentation tests with a Berkovich indenter at a peak load of 100 mN and a constant strain rate of 0.05 s^{-1}. Note that, in this study, no noticeable influence of either the GB types or the grain orientations on nanoindentation results was found, which is in agreement with literature data of alloy 690 showing a weak dependence of nanohardness on the grain orientations [9], grain size [9], and GB types [10].

Measured nanohardness values are summarized in Fig. 2 where inset image showing impressions located on GB and in GI is also provided. It is obvious that the hardness of the GB is always higher than that of GI in any specimen. There can be two possible contributions to the higher hardness of the GB. On one hand, the GBs are not only the obstacles of dislocation motion but also strong sources of dislocations (especially, geometrically necessary dislocations, GNDs). Therefore, high hardness of the GBs should be closely associated with Taylor hardening by high-density dislocations near GBs during nanoindentation [11]. On the other hand, intergranular $M_{23}C_6$ precipitates additionally enhances the GB hardness by particle strengthening mechanisms such as Orowan bowing and cutting mechanism [12,13].

An important feature in the figure is that the difference in nanohardness, ΔH, between the GB and GI (i.e., amount of GBs' contributions) remains almost constant and is almost independent of aging time, which can be explained by the lack of additional precipitate nucleation and the slow coarsening of pre-existing precipitates during aging (as mentioned above). No pronounced change in the GI hardness in Fig. 2 may indicate that the alloying elements for solid-solution strengthening in the matrix (mainly chromium) were not consumed for the GB carbides formation during aging, which supports the lack of precipitates nucleation during aging.

During nanoindentation tests with a spherical indenter, load–displacement (P–h) curves often exhibit a sudden displacement excursion (referred to as 'pop-in') at relatively low load. Fig. 3 shows a representative example of the P–h curve recorded during a spherical indentation, in which several pop-ins are observed. It is well accepted that the 'first' pop-in is associated with the onset of plasticity, i.e., elastic-to-plastic transition or yielding [14,15]. The deformation prior to the first pop-in is purely elastic (which is supported by the fact that the loading curve is fully recoverable upon unloading, as shown in the inset of Fig. 3) and thus the elastic P-h behavior follows the Hertzian contact theory [16]:

$$P = \frac{4}{3} E_r R^{\frac{1}{2}} h^{\frac{3}{2}} \tag{2}$$

where R is the tip radius (68.5 μm in this study), and E_r is the reduced modulus, which is given by $1/E_r = (1 - \nu_s^2)/E_s + (1 - \nu_i^2)/E_i$. In this expression, E is the Young's modulus and ν is Poisson's ratio, with the subscripts s and i indicating the sample and the indenter. For the diamond tip employed in the studies, E_i = 1141 GPa and ν_i = 0.07. By fitting the loading segment of the P-h curve by Eq. (2) (see Fig. 3) [16], the indentation modulus of the sample, $E_s/(1 - \nu_s^2)$ (that can be easily calculated from E_r), was determined as ~225 GPa. The value is in good agreement with literature data (~232 GPa based on E_s = 211 GPa and ν_s = 0.289 [17]).

As the first pop-in event is caused by the yielding, the maximum shear stress at the first pop-in load, τ_{max}, represents the critical shear yield strength. For Hertzian contact, the τ_{max} occurs at a distance approximately half the contact radius directly below contact on the axis of symmetry. The magnitude of this shear stress is given by [16]:

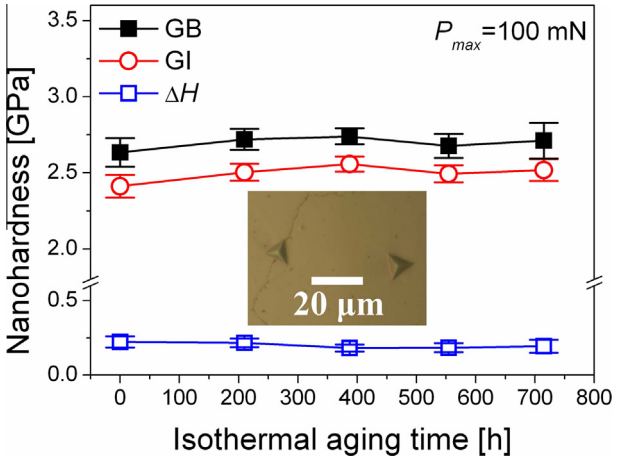

Fig. 2. Summary of measured nanohardness values. ΔH is the hardness difference between GB and GI. The inset image shows representative optical microscopy images of nanoindentations located on GB and in GI.

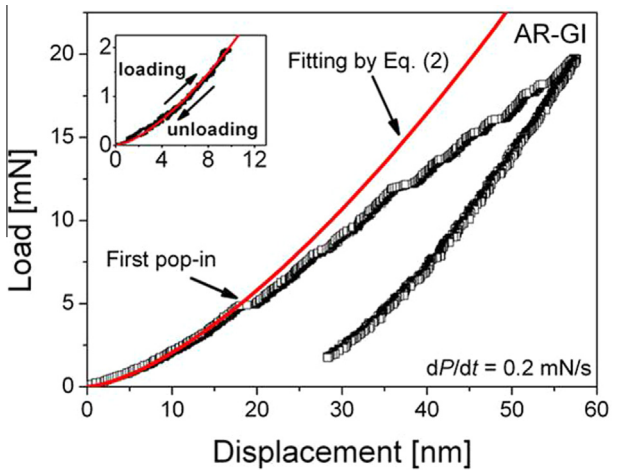

Fig. 3. Typical example of the P–h curve from spherical nanoindentation test; this example is for GI of AR sample. Insert shows the fully elastic curve obtained at low load.

$$\tau_{max} = 0.31 \left(\frac{6 P_{cri} E_r^2}{\pi^3 R^2} \right)^{\frac{1}{3}} \tag{3}$$

where P_{cri} is the critical load at the first pop-in event.

Fig. 4 presents the plot of the τ_{max} for the GB and GI as a function of aging time. If one may consider a typical wide distribution of the τ_{max} for a given condition (conceivably due to the nature of inhomogeneous distribution of dislocation sources [9,18]), the aging-induced variations in τ_{max} for both the GI and GB indentations are almost negligible. This is mainly owing to the absence of dramatic microstructural change during aging, being similar to nanohardness change in Fig. 2. However, the average τ_{max} for the GI is higher than that of the GB, which is opposite to the trend of nanohardness (i.e., nanohardness of the GB is higher than that of the GI). This difference can be explained by the different natures between plastic flow (for nanohardness) and yielding (for pop-in) during nanoindentation [18]. The former is governed by interactions between moving dislocations and crystalline defects (e.g., the GBs and other dislocations) and thus a material is seriously strengthened by the presence of the GBs, whereas the latter is controlled by the dislocation nucleation underneath the indenter and can occur more easily (i.e., τ_{max} is decreased) in the vicinity of GBs that are strong sources of dislocation nucleation [10].

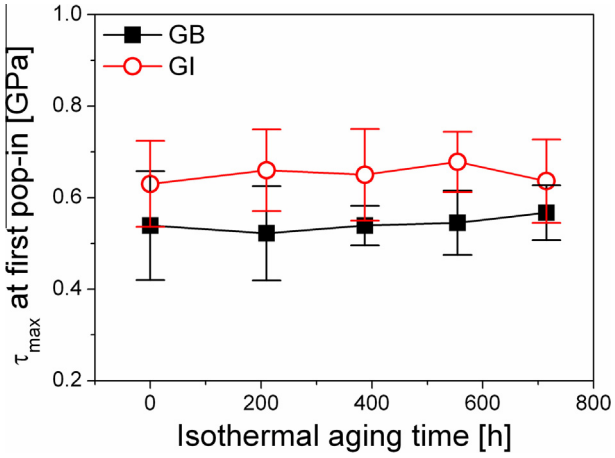

Fig. 4. Summary of the estimated maximum shear stress at the first pop-in.

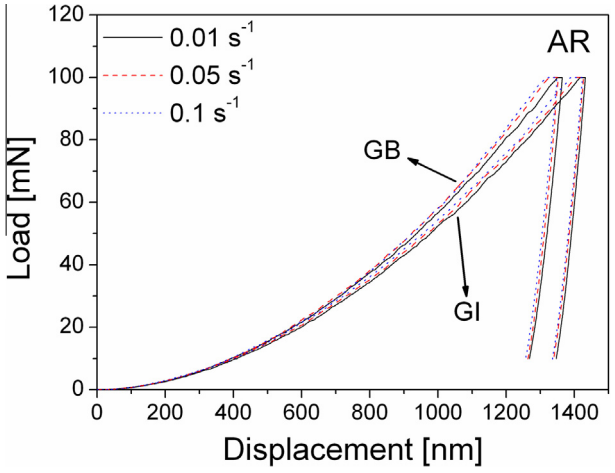

Fig. 5. Representative *P–h* curves of AR specimen recorded under three different indentation strain rates.

Now, we turn our attention to two key signatures for thermally-activated, stress-assisted plastic deformation mechanism; strain rate sensitivity (SRS) m and activation volume V^*, which provide both a quantitative rate-dependency of flow stress and a clue for the deformation mechanisms. In nanoindentation, the SRS m of material can be experimentally obtained from the relation between hardness H and strain rate $\dot{\varepsilon}$ [19]:

$$m = \frac{\partial \ln H}{\partial \ln \dot{\varepsilon}}. \tag{4}$$

The nanoindentation strain rate is defined as the instantaneous descent rate of the indenter divided by the depth, $\dot{\varepsilon} = (\mathrm{d}h/\mathrm{d}t)/h$ [20]. The activation volume V^* can be expressed as [21]:

$$V^* = 3\sqrt{3}kT\left(\frac{\partial \ln \dot{\varepsilon}}{\partial H}\right) = \frac{3\sqrt{3}kT}{mH} \tag{5}$$

where k is the Boltzmann's constant, and T is the absolute temperature.

The nanoindentation tests for determining SRS were performed on the AR and 715-h-aged (i.e., the most aged) specimens with a Berkovich indenter at a peak load of 100 mN and at three different constant strain rates: 0.01, 0.05 and 0.1 s^{-1}. Fig. 5 shows typical *P-h* response of AR specimen. A detectable effect of indentation strain rate on the curve is evident, that is, with increasing strain rates, the h_{max} decreases and thus nanohardness increases.

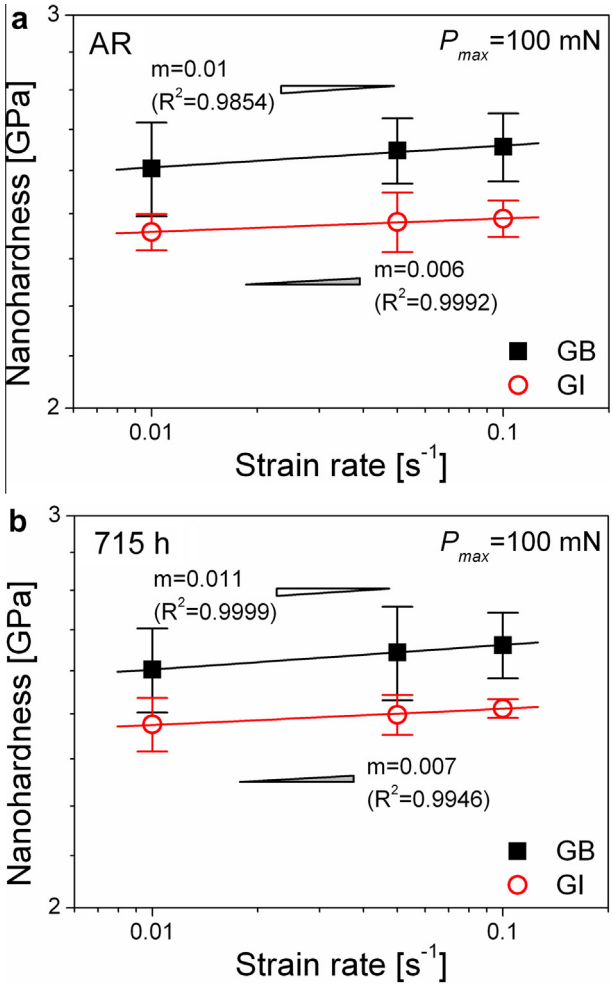

Fig. 6. Double logarithmic plots of hardness versus strain rate (for AR and 715-h-aged specimens). Each slope indicates the m value.

Table 1
Strain rate sensitivity m and activation volume V^* of AR and 715-h-aged samples.

	AR		715 h aged	
	GB	GI	GB	GI
m	0.01	0.006	0.011	0.007
V^*	~54b^3	~94b^3	~48b^3	~78b^3

The m estimated from Fig. 6 and the corresponding activation volume V^* are listed in Table 1. The V^* values are expressed in terms of b^3, where b is the Burgers vector and ~0.249 nm for nickel [22]. While there is no significant difference in SRS between AR and 715-h-aged specimen (as expected from the lack of serious aging-induced microstructural changes), the m is largely enhanced for GB.

The m for the GI is 0.006 and 0.007 for AR and 715-h-aged specimens respectively, which is very close to the literature value of 0.005 in coarse-grained Ni estimated through nanoindentation tests [23]. One possible predominant rate-limiting mechanism is cross-slip by screw dislocations which can escape from their locked positions to change slip planes. Activation volume of the cross-slip in coarse-grained fcc metals is known to be ~10–100b^3 [24], which is in agreement with our values. In the area where GBs are involved, the GBs may provide additional active deformation mechanisms such as dislocation generation/emission [25],

leading to increase in m (~0.01) and decrease in V^* (~80–90b^3) compared to those in the GI ($m \sim 0.006$ and $V^* \sim 50b^3$).

4. Summary

In this study, we explored the nanoindentation behavior of the GBs and GI in the TT 690 alloy specimens that were isothermally aged for four different times (for simulating the 20–80 years operation under power plant condition). While no pronounced aging-induced degradation was detected, the GBs show reproducible differences in nanohardness (plastic flow), pop-in stress (yielding), and strain-rate dependency of hardness from those from GIs. The results are discussed in terms of the roles of dislocations in the mechanism for each behavior.

Acknowledgement

This research was supported by the Human Resources Development of the Korea Institute of Energy Technology Evaluation and Planning (KETEP) grant funded by the Korea government Ministry of Trade, Industry and Energy (No. 20114010203020).

References

[1] D.L. Harrod, R.E. Gold, R.J. Jacko, Alloy optimization for PWR steam generator heat-transfer tubing, JOM 53 (2001) 14–17.
[2] J.J. Kai, G.P. Yu, C.H. Tsai, M.N. Liu, S.C. Yao, The effect of heat treatment on the chromium depletion, precipitate evolution, and corrosion resistance of INCONEL alloy 690, Metall. Trans. A 20 (1989) 2057–2067.
[3] E.A. West, G.S. Was, IGSCC of grain boundary engineered 316L and 690 in supercritical water, J. Nucl. Mater. 392 (2009) 264–271.
[4] M. Casales, V.M. Salinas-Bravo, A. Martinez-Villafane, J.G. Gonzalez-Rodriguez, Effect of heat treatment on the stress corrosion cracking of alloy 690, Mater. Sci. Eng. A 332 (2002) 223–230.
[5] T.M. Angeliu, G.S. Was, Behavior of grain boundary chemistry and precipitates upon thermal treatment of controlled purity alloy 690, Metall. Trans. A 21 (1990) 2097–2107.
[6] J.-i. Jang, S. Shim, S.-i. Komazaki, T. Honda, A nanoindentation study on grain-boundary contributions to strengthening and aging degradation mechanisms in advanced 12 Cr ferritic steel, J. Mater. Res. 22 (2007) 175–185.
[7] S.A. Sajjadi, S. Nategh, R.I.L. Guthrie, A study of microstructure and mechanical properties of high performance Ni-base superalloy GTD-111, Mater. Sci. Eng. 325 (2002) 484–489.
[8] W.C. Oliver, G.M. Pharr, An improved technique for determining hardness and elastic modulus using load and displacement sensing indentation experiments, J. Mater. Res. 7 (1992) 1564–1583.
[9] J.J. Marra, Relationship of grain boundary structure and mechanical properties of inconel 690. Thesis, MIT, June 2009.
[10] W. Herbert, B. Yildiz, K.J. Van Vliet, Mater. Res. Soc. Symp. Proc. Vol. 1297, Materials Research Society, 2011, doi: 10.1557/opl.2011.
[11] G.I. Taylor, Plastic strain in metals, J. Inst. Metals 62 (1938) 307–324.
[12] J.-H. Oh, B.-G. Yoo, I.-C. Choi, M.L. Santella, J.-i. Jang, Influence of thermo-mechanical treatment on the precipitation strengthening behavior of Inconel 740, a Ni-based superalloy, J. Mater. Res. 26 (2011) 1253–1259.
[13] J. Moon, S. Kim, J.-i. Jang, J. Lee, C. Lee, Orowan strengthening effect on the nanoindentation hardness of the ferrite matrix in microalloyed steels, Mater. Sci. Eng. A 487 (2008) 552–557.
[14] I.-C. Choi, Y. Zhao, Y.-J. Kim, B.-G. Yoo, J.-Y. Suh, U. Ramamurty, J.-i. Jang, Indentation size effect and shear transformation zone size in a bulk metallic glass in two different structural states, Acta Mater. 60 (2012) 6862–6868.
[15] J.-i. Jang, H. Bei, P.F. Becker, G.M. Pharr, Experimental analysis of the elastic-plastic transition during nanoindentation of single crystal alpha-silicon nitride, J. Am. Ceram. Soc. 95 (2012) 2113–2115.
[16] K.L. Johnson, Contact Mechanics, Cambridge University Press, Cambridge, 1985.
[17] INCONEL® alloy 690, Special Metals Corporation, Huntington (WV).<http://www.specialmetals.com/products/inconelalloy690>(updated 09.10.09)
[18] T. Ohmura, K. Tsuzaki, Plasticity initiation and subsequent deformation behavior in the vicinity of single grain boundary investigated through nanoindentation technique, J. Mater. Sci. 42 (2007) 1728–1732.
[19] M.J. Mayo, W.D. Nix, A micro-indentation study of superplasticity in Pb, Sn, and Sn-38 wt% Pb, Acta Metall. 36 (1988) 2183–2192.
[20] B.N. Lucas, W.C. Oliver, Indentation power-law creep of high-purity indium, Metall. Mater. Trans. A 30 (1999) 601–610.
[21] H. Conrad, in: V.F. Zackey (Ed.), High-Strength Materials, John Wiley & Sons, New York, 1965.
[22] I.E. Murr, Interfacial Phenomena in Metals and Alloys, Addison-Wesley, Reading, MA, 1975.
[23] D. Pan, T.G. Nieh, M.W. Chen, Strengthening and softening of nanocrystalline nickel during multistep nanoindentation, Appl. Phys. Lett. 88 (2006) 161922.
[24] D. Caillard, J.L. Martin, Thermally Activated Mechanisms in Crystal Plasticity, Pergamon, Amsterdam, 2003.
[25] I.-C. Choi, Y.-J. Kim, M.-Y. Seok, B.-G. Yoo, J.-Y. Kim, Y. Wang, J.-i. Jang, Nanoscale room temperature creep of nanocrystalline nickel pillars at low stresses, Int. J. Plast. 41 (2013) 53–64.